

Magnetoelectric Effects in Complex Oxides with Competing Ground States

By Hajo J. A. Molegraaf, Jason Hoffman, Carlos A. F. Vaz,* Stefano Gariglio, Dirk van der Marel, Charles H. Ahn, and Jean-Marc Triscone

The drive to develop materials with new multifunctional capabilities has rekindled interest in multiferroics—systems which are characterized by the simultaneous presence of, and coupling between, magnetic and electric order parameters. In naturally occurring multiferroics the magnetoelectric coupling is often weak, and new classes of artificially structured composite materials that combine dissimilar magnetic and ferroelectric systems are being developed to optimize order parameter coupling.^[1–6] Here, we describe direct, charge-mediated magnetoelectric coupling in a heterogeneous multiferroic that takes advantage of the sensitivity of a strongly correlated magnetic system to competing electronic ground states. Using magneto-optic Kerr effect magnetometry, we observe large magnetoelectric coupling in ferroelectric/lanthanum manganite heterostructures, including electric field-controlled on/off switching of magnetism. These results open a new vista for the development of novel magnetoelectric devices with large charge coupling between electric and magnetic degrees of freedom.

Doped lanthanum manganites are complex oxides characterized by a strong interplay between electron transport, magnetism, and crystal lattice distortions, leading to a rich variety of electronic behavior, including magnetic and charge-ordered states, colossal magnetoresistance (CMR), and a diversity of electron transport behavior. Underlying the competition between these ground states is the prominent role of charge in double exchange, hopping, and orbital overlap.^[7,8] To date, controlling charge as a parameter has most often been achieved using chemical doping, which is robust, and permanent. An alternative approach to

modulate carrier density is to use an electrostatic field,^[9–15] which has been used successfully to modulate charge-dependent phenomena, including superconductivity^[16] and dilute magnetic semiconducting behavior.^[12,13,17] In these systems, the nature of the electron correlations results in a strong sensitivity of the material properties to the charge-carrier concentration.

Magnetism has also been controlled at interfaces using field effects. Magnetotransport measurements (planar and anomalous Hall effect, magnetoresistance, resistance) indicate large changes in critical temperature,^[12,13,18–20] while changes in coercivity have also been observed.^[14] Moreover, magnetoelectric effects at interfaces have been predicted to arise from spin density accumulation in metallic ferromagnet/ferroelectric structures, induced by charge screening of the electric field.^[5] These experimental and theoretical results point to the potential of these types of structures for nanostructured multiferroics.

Here, we demonstrate a large charge-driven magnetoelectric coupling effect in a Sr-doped lanthanum manganite/ferroelectric composite structure resulting from direct control of magnetism via charge carrier density. This approach has the advantage that its physical mechanism is transparent and the size of the effect can be quantified and understood qualitatively within the double exchange model, in particular the observed variation of the magnetic moment and critical temperature with charge carrier concentration. This approach is an alternative to electroelastic modulation of the magnetic properties of magnetic/ferroelectric composites, where magnetoelectric coupling is achieved through changes in magnetic anisotropy and remanent magnetization via strain.^[1,21] The converse effect, in which the electric polarization is modulated by a magnetic field, has also been demonstrated.^[1,2,22,23]

In this study, we use off-axis magnetron sputtering to grow a continuous 250 nm $\text{PbZr}_{0.2}\text{Ti}_{0.8}\text{O}_3$ /4.0 nm $\text{La}_{0.8}\text{Sr}_{0.2}\text{MnO}_3$ bilayer structure on a $\text{SrTiO}_3(001)$ single crystal (see Fig. 1a). We chose $\text{La}_{0.8}\text{Sr}_{0.2}\text{MnO}_3$ (LSMO) since the bulk compound lies near the boundary between metallic and insulating ferromagnetic ground states; the magnetic Curie temperature occurs at 300 K.^[24] In field-effect structures the induced electric polarization at the gate oxide creates a surface charge density at the interface, which is screened by an equal number of charge carriers of the opposite sign, changing the effective doping of the system. One challenge with the field-effect approach here is the nearly metallic hole-doping level of LSMO (10^{21} holes cm^{-3}), which results in a screening length that is only a few angstroms; ultrathin, atomically flat ferromagnetic layers are therefore required in order to observe a measurable effect. To provide the electric field, we used the spontaneous electric polarization of $\text{PbZr}_{0.2}\text{Ti}_{0.8}\text{O}_3$

[*] Dr. C. A. F. Vaz
Becton Center
Yale University
P.O. Box 208284, New Haven, CT 06520-8284 (USA)
E-mail: carlos.vaz@yale.edu

Dr. C. A. F. Vaz, J. Hoffman, Prof. C. H. Ahn
Department of Applied Physics
Yale University
New Haven, CT 06520 (USA)

Dr. C. A. F. Vaz, J. Hoffman, Prof. C. H. Ahn
Center for Research on Interface Structures and Phenomena (CRISP)
Yale University
New Haven, CT 06520 (USA)

Dr. H. J. A. Molegraaf, Dr. S. Gariglio, Prof. D. van der Marel,
Prof. J.-M. Triscone
DPMC, University of Geneva, 24 Quai Ernest Ansermet
1211 Geneva 4 (Switzerland)

DOI: 10.1002/adma.200900278

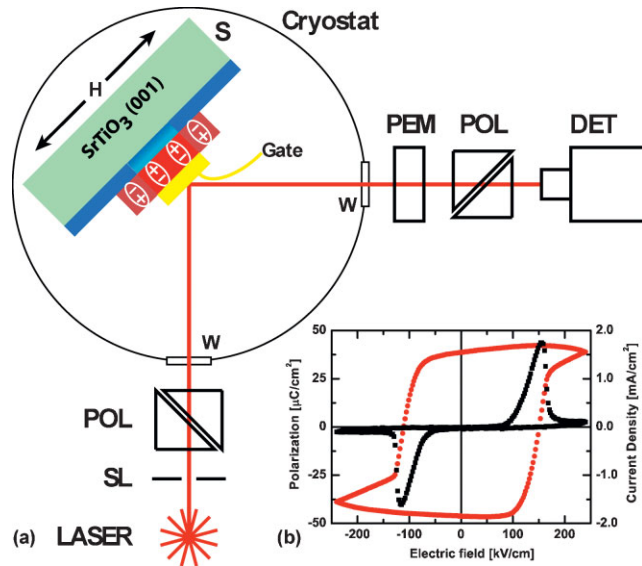


Figure 1. a) Schematic diagram of the PZT (red)/LSMO (blue)/SrTiO₃ (001) structure (S) and of the measurement geometry. An s-polarized focused laser beam is reflected off the sample surface towards a photoelastic modulator (PEM), a Glan-Thompson analyzer (POL) and a photodiode detector (DET). A Au (yellow) gate electrode (Gate) is used to switch the PZT polarization in the active area of the device. (SL: iris collimator, W: cryostat window.) **H** represents the direction of the applied magnetic field. b) Room temperature *P*–*E* response (red circles, left axis) showing a square hysteresis loop, with a remanent polarization of 45 $\mu\text{C cm}^{-2}$. The displacement current as the applied electric field is ramped at 1.6 $\text{MV cm}^{-1} \text{s}^{-1}$ (black squares, right axis) exhibits a sharp increase at the PZT switching field and indicates a low leakage current.

(PZT), which can generate polarizations of the order of 50 $\mu\text{C cm}^{-2}$, much larger than the breakdown field of SiO₂. For the bilayer structures, X-ray diffraction reveals that the PZT is *c*-axis oriented, with the polarization lying perpendicular to the film surface.^[18,25] The polarization can be switched by applying a voltage across the PZT layer, using a gold top electrode and the LSMO layer as the bottom electrode. Polarization–electric field (*P*–*E*) hysteresis measurements reveal a square loop with a remanent polarization of $\sim 45 \mu\text{C cm}^{-2}$ (Fig. 1b). Clear peaks are observed in the displacement current at the coercive field, confirming polarization switching of PZT (Fig. 1b) with a low leakage-current characteristic.

To probe the local magnetic state of the LSMO as a function of the PZT polarization state, we employ magneto-optic Kerr effect (MOKE) magnetometry. In this technique, the sample magnetization gives rise to changes in the polarization of light reflected off the surface. We measure the Kerr rotation and ellipticity, both of which are proportional to the magnetization (although different in amplitude). For the reflection geometry used here, optical effects originating from the birefringence of the PZT and SrTiO₃ substrate (which becomes tetragonal below ~ 100 K) are negligible, as corroborated by magneto-optic calculations. We used ac modulation techniques to increase the sensitivity of the magnetometer (see Experimental). The magnetic field is applied in the plane of the sample, the same direction as that of the remanent magnetization.

In Figure 2, we show how the magnetization of the structure evolves as a function of temperature and ferroelectric polariza-

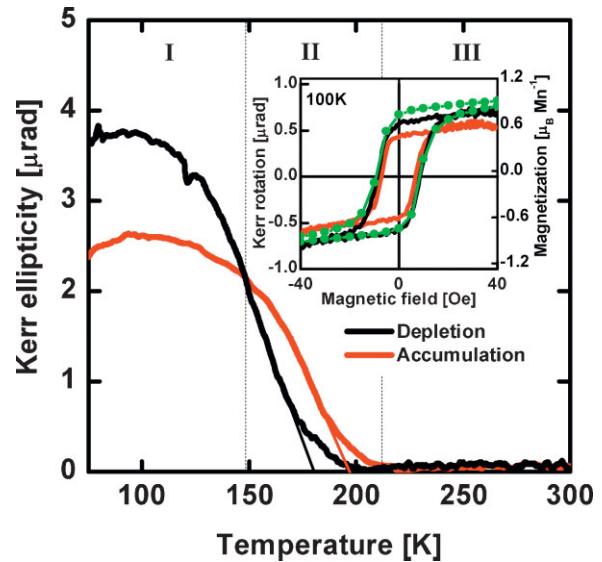


Figure 2. Temperature dependence of the LSMO magnetization for the two polarization states of the PZT layer. A shift in T_c of about 20 K is observed. The inset shows quasi-static *M*–*H* loops measured at 100 K for the accumulation and depletion states. Full lines: MOKE data; symbols: SQUID data (depletion state). The γ -axis corresponds to the magnetic moment of the 4 nm LSMO film obtained from SQUID magnetometry, which is used to calibrate the MOKE signal.

tion. The red and black curves correspond to the states where the ferroelectric adds and removes charges from the magnetic LSMO layer; these are termed the accumulation and depletion states, respectively. We distinguish three different temperature regimes for the magnetization curves. At high temperatures (region III, $T > 212$ K) we find that LSMO is in a paramagnetic state for both polarization states and shows no magnetic response. For intermediate temperatures (region II, $147 < T < 212$ K), we observe a vertical and horizontal split in the magnetization curves, where the accumulation state becomes magnetic at higher temperatures and has a larger magnetization than in the depletion state. A crossover in behavior is observed at 147 K (region I), where a reversal in the relative position of the magnetization curves occurs: the magnetization for the depletion state becomes larger than that for the accumulation state. This region is also characterized by the gradual increase of the magnetization towards a constant ground-state value.^[26]

To better understand the evolution of the observed behavior, we measured magnetic hysteresis loops at several temperatures for the two polarization states of the PZT layer. At low temperatures, the *M*–*H* curves show that the LSMO magnetization switches hysteretically between oppositely magnetized states, confirming the ferromagnetic ordering of the LSMO for the chosen chemical and field-effect dopings (Fig. 2, inset). The *M*–*H* loops also show that in region I the magnetization of the LSMO in the depletion state is higher than that in the accumulation state. We also find a change in coercivity for the two doping levels.^[14] In region II, the opposite behavior is observed, as expected from the higher T_c for the accumulation state.^[15,18]

Analysis of the magnetization data of Figure 2 reveals that the two *M*–*T* curves collapse onto each other after a suitable vertical rescaling and a temperature shift of 20 K. This result shows that,

while there is a substantial change in T_c and saturation magnetization for the accumulation and depletion states, the normalized M - T behavior is largely unaffected by the change in carrier concentration. The critical temperatures are estimated as 179 and 197 K for the depletion and accumulation states, respectively, from linear extrapolations to zero magnetization near the critical region (Fig. 2). The lower T_c for the depletion state is consistent with the bulk phase diagram of the doped lanthanum manganites in the ferromagnetic regime, where T_c increases with doping level.^[27,28]

We now discuss the interpretation of the individual regions I and II in more detail. First, we note that the decrease in the ground state magnetization with increase in the doping level, observed in region I of Figure 2 and also in the hysteresis loops, may at first sight seem surprising since it implies that the material with the higher T_c has a lower magnetization. However, this trend is exactly what is expected in the ferromagnetic phase of the bulk CMR manganites,^[27,29] where the magnetic moment varies with hole concentration, x , as $(4-x)\mu_B$ per Mn (where μ_B is the Bohr magneton): as the hole concentration (doping) increases, a larger fraction of the Mn cations change from an $S=2$ (Mn^{3+}) to an $S=3/2$ (Mn^{4+}) spin state. However, while the trend is the expected one, the change in the magnetic moment seems somewhat too large to be explained only by band-filling effects. That is reflected in the notation of Spaldin and co-workers,^[5] where we obtain a large ratio of induced spin to charge density surface of $\eta \approx 2$.

That a simple band-filling model fails to describe the electronic behavior of these strongly correlated materials is not surprising, given the sensitivity of the electronic and magnetic ground state to electron-electron correlations and the presence of inhomogeneities in these materials. Changes in the carrier density may favor nonparallel spin arrangements or changes in the valence state of the Mn. Other possible mechanisms that could lead to an enhanced effect could be related to Sr segregation to the interface layer, which could favor an antiferromagnetic spin coupling for the accumulation state,^[30,31] or changes in valency of a spin-coupled Mn^{3+} to a noncoupled, paramagnetic Mn^{2+} , whose presence in LSMO thin films has been suggested in recent experimental studies.^[32,33]

This competition between ground states and their sensitivity to the charge-carrier density can be exploited to achieve large magnetoelectric couplings driven directly by charge and electric field. A striking illustration of this magnetoelectric coupling is given in Figure 3, where we show the magnetic response of the system as a function of the applied electric field, showing abrupt modulation of the LSMO magnetization as the PZT polarization switches. In contrast to traditional M - H and P - E loops, which reveal how an individual ferroic (magnetic, ferroelectric) material responds to its natural stimulus (magnetic field, electric field), this M - E loop demonstrates cross-coupling between ferroic ground states, showing a hysteretic magnetic response as a function of electric field. In our system, the magnetoelectric coupling is achieved via modulation of the charge-carrier concentration and is directly linked to the gate oxide surface bound charge, where the relevant coupling is between the magnetic moment and the electric polarization.^[34] The figure of merit that characterizes the size of the magnetoelectric coupling in our system is $\Delta M/\Delta E$; using the width of the M - E hysteresis,

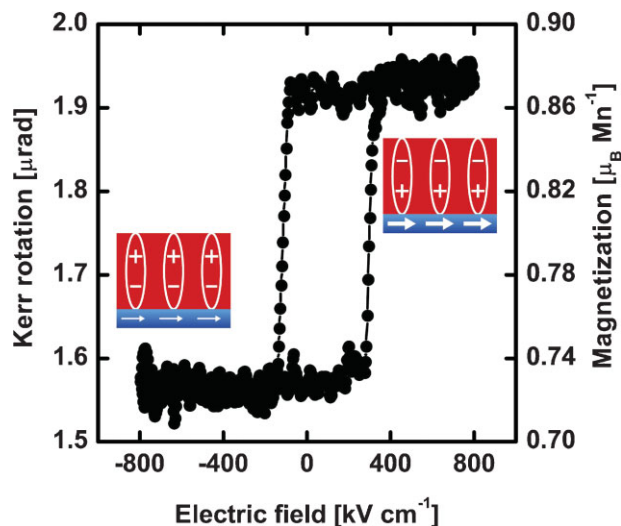


Figure 3. Magnetolectric hysteresis curve at 100 K showing the magnetic response of the PZT/LSMO system as a function of the applied electric field. The two magnetization values correspond to modulation of the magnetization of the LSMO layer. Insets represent the magnetic and electric states of the LSMO and PZT layers, respectively. The size of the arrows indicates qualitatively the magnetization amplitude.

we obtain $\Delta M/\Delta E = 0.8 \times 10^{-3}$ Oe cm V^{-1} at 100 K (1 Oe = $1000/4\pi$ A m^{-1}). Since the effect reported here is an interfacial effect, this value of $\Delta M/\Delta E$ is specific to the particular thicknesses in our system. For magneto- and piezoelastically coupled composites, values up to 25×10^{-3} Oe cm V^{-1} have been reported.^[1,21,35] In these kinds of composites, the magnetoelectric coupling is achieved through changes in strain, while here we induce a change in magnetism via a charge-mediated mechanism.^[36] A direct comparison to bulk materials is difficult because of the interfacial nature of the effect, but we note here that the values for the linear magnetoelectric coupling coefficient, α , for homogeneous multiferroics are $\sim 10^{-5}$ Oe cm V^{-1} . We also note that the observed magnetoelectric coupling effect reported here is hysteretic, nonlinear, and persistent.^[22]

We next examine the magnetic response of the system in region II, where the change in magnetism is most sensitive to the two polarization states of the ferroelectric. We consider various configurations of the applied electric and magnetic fields. For a range of temperatures close to the critical interval, only the accumulation state orders magnetically, and the magnetism in the LSMO layer can be turned on and off reversibly, as shown in Figure 4 for $T = 197$ K. The figure shows that when the PZT is polarized downwards ($t = 0$), the LSMO is in a nonmagnetic state (zero Kerr ellipticity). The system becomes magnetic upon switching of the PZT polarization upwards at $t = 7$ min (accumulation state). When the PZT polarization is subsequently switched again to the down state ($t = 15$ min), the LSMO reverts to its nonmagnetic state, showing reversible and reproducible control of the magnetism in LSMO through an applied electric field.^[37] When the ac magnetic field is turned off at $t = 25$ min, no changes in the Kerr signal from the background baseline are observed, both for the depletion ($t = 25$ min) and accumulation ($t = 32$ min) states. (This zero-field measurement sets the baseline for zero magnetization.)

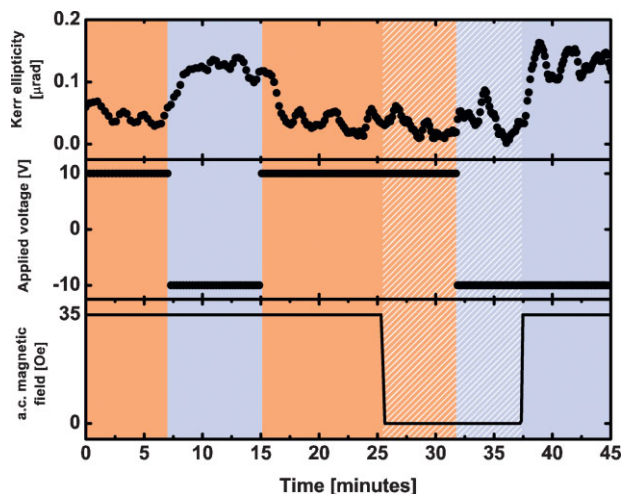


Figure 4. Magnetic response of the PZT/LSMO bilayer at 197 K for both polarization states of PZT, showing the control of magnetism with applied electric field (middle panel). The color represents the polarization state of PZT, corresponding to depletion (orange, +10V) and accumulation (blue, -10V) states. The bottom panel shows the a.c. excitation field amplitude. The Kerr signal at zero a.c. field (hatched area) corresponds to the background signal of the instrument (zero magnetization).

In summary, we have demonstrated reversible electric control of the magnetic properties of a CMR manganite, including the onset of ferromagnetic order and modulation of the magnetization amplitude, via direct magnetic measurements. We show that changes in T_c of the order of 20 K are achievable in doped lanthanum manganite thin films via magnetoelectric coupling. The magnetism of the LSMO layer can be switched on or off by means of an applied electric field, constituting a magnetoelectric coupling in composite multiferroic systems based on an electronic charge-modulation mechanism. We obtain a magnetoelectric coupling coefficient that is much larger than those of intrinsic multiferroic systems. Optimization of the materials employed, such as the use of a ferroelectric material with a smaller electric coercive field or a magnetic material with a doping level in closer proximity to a magnetic phase transition, may be able to yield structures with a larger magnetoelectric response. In addition, because this carrier-based mechanism alters the band filling of the magnetic material (majority and minority bands), this approach can be applied to modulate spin polarization of itinerant magnetic systems, as proposed by Spaldin and co-workers.^[5]

Experimental

A continuous 250 nm $\text{Pb}(\text{Zr}_{0.2}\text{Ti}_{0.8})\text{O}_3/4$ nm $\text{La}_{0.8}\text{Sr}_{0.2}\text{MnO}_3/\text{SrTiO}_3(001)$ bilayer structure was grown by off-axis magnetron sputtering, using the growth method and conditions described in [18]. Atomic force microscopy and X-ray scattering measurements were carried out to determine the surface and crystalline quality of the PZT/LSMO bilayer structure. On this structure, a $400 \times 600 \mu\text{m}^2$ gold contact (~ 10 nm thick) was deposited, which serves as a gate electrode. The size of the contact was made large enough to accommodate the focused laser beam for the magneto-optic Kerr effect (MOKE) magnetometry measurements. The gold layer is thin enough to be transparent to the laser beam (~ 1 mW power, $\lambda = 633$ nm). The attenuation length of light in LSMO is

~ 100 – 200 nm at 633 nm wavelength, and thus the MOKE measurements access the whole of the 4 nm magnetic film. Piezoelectric force microscopy was performed both on as-grown areas of the sample and in the region under the Au contact (which was removed prior to this particular measurement), and demonstrates the uniformity of the electric polarization of PZT upon switching.

For the magnetic measurements, the sample was placed in a high vacuum cryostat with optical apertures for longitudinal MOKE measurements. The light polarization was modulated using a photoelastic modulator operating at 50 kHz, while the signal at the detector was fed to a lock-in amplifier locked either to the fundamental harmonic (signal proportional to the Kerr ellipticity) or to the second harmonic (signal proportional to the Kerr rotation) [38]. Although both quantities are proportional to the magnetization, they differ in amplitude. The magnetic field was generated by a coreless electromagnet that provides magnetic field amplitudes of up to 30 Oe at room temperature and up to 80 Oe at 20 K in the frequency range from 0 to ~ 120 Hz. Two types of MOKE measurements were performed: (i) in the d.c. mode, the Kerr rotation or ellipticity is measured against a slowly varying (quasi-static) magnetic field (0.005 Hz), yielding ordinary M - H characteristics. (ii) In the a.c. mode, an oscillating magnetic field (12 Hz) is applied to the sample, and the Kerr rotation or ellipticity is measured by a second lock-in amplifier locked at the field excitation frequency. In these measurements, the output signal is proportional to the saturation magnetization amplitude averaged over many field cycles. The latter technique has the advantage that the non-magnetic optical contributions are automatically filtered from the output signal. With this arrangement, the Kerr rotation and ellipticity are measured with a precision of better than 50 nrad.

Acknowledgements

Work at Yale supported by NSF MRSEC DMR 0520495, ONR, and NRI-INDEX. Work at Geneva supported by the Swiss National Science Foundation through the “National Center of Competence in Research Materials with Novel Electronic Properties—MaNEP” and Division II programs, and the EU Strep project Macomufi.

Received: January 24, 2009
Published online:

- [1] M. Fiebig, *J. Phys. D: Appl. Phys.* **2005**, *38*, R123.
- [2] W. Eerenstein, N. D. Mathur, J. F. Scott, *Nature* **2006**, *442*, 759.
- [3] R. Ramesh, N. A. Spaldin, *Nat. Mater.* **2007**, *6*, 21.
- [4] M. Gajek, M. Bibes, S. Fusil, K. Bouzehouane, J. Fontcuberta, A. Barthélémy, A. Fert, *Nature Mater.* **2007**, *6*, 296.
- [5] J. M. Rondinelli, M. Stengel, N. A. Spaldin, *Nat. Nanotechnol.* **2008**, *3*, 46.
- [6] Y.-H. Chu, L. W. Martin, M. B. Holcomb, M. Gajek, S.-J. Han, Q. He, N. Balke, C.-H. Yang, D. Lee, W. Hu, Q. Zhan, P.-L. Yang, A. Fraile-Rodríguez, A. Scholl, S. X. Wang, R. Ramesh, *Nat. Mater.* **2008**, *7*, 478.
- [7] A. Moreo, S. Yunoki, E. Dagotto, *Science* **1999**, *283*, 2034.
- [8] Y. Tokura, Y. Tomioka, *J. Magn. Magn. Mater.* **1999**, *200*, 1.
- [9] C. H. Ahn, J.-M. Triscone, J. Mannhart, *Nature* **2003**, *424*, 1015.
- [10] C. H. Ahn, A. Bhattacharya, M. Di Venira, J. N. Eckstein, C. D. Frisbie, M. E. Gershenson, A. M. Goldman, I. H. Inoue, J. Mannhart, A. J. Millis, A. F. Morpurgo, D. Natelson, J.-M. Triscone, *Rev. Mod. Phys.* **2006**, *78*, 1185.
- [11] T. Venkatesan, D. C. Kundaliya, T. Wu, S. B. Ogale, *Phil. Mag. Lett.* **2007**, *87*, 279.
- [12] H. Ohno, D. Chiba, F. Matsukura, T. Omiya, E. Abe, T. Dietl, Y. Ohno, K. Ohtani, *Nature* **2000**, *408*, 944.
- [13] D. Chiba, M. Yamanouchi, F. Matsukura, H. Ohno, *Science* **2003**, *301*, 943.
- [14] M. Weisheit, S. Fähler, A. Marty, Y. Souche, C. Poinsignon, D. Givord, *Science* **2007**, *315*, 349.

- [15] T. Kanki, H. Tanaka, T. Kawai, *Appl. Phys. Lett.* **2006**, *89*, 242506-1.
- [16] C. H. Ahn, S. Gariglio, P. Paruch, T. Tybell, L. Antognazza, J.-M. Triscone, *Science* **1999**, *284*, 1152.
- [17] I. Stolichnov, S. W. E. Rieder, H. J. Trodahl, N. Setter, A. W. Rushforth, K. W. Edmonds, R. P. Campion, C. T. Foxon, B. L. Gallagher, T. Jungwirth, *Nat. Mater.* **2008**, *7*, 464.
- [18] X. Hong, A. Posadas, A. Lin, C. H. Ahn, *Phys. Rev. B* **2003**, *68*, 134415-1.
- [19] X. Hong, A. Posadas, C. H. Ahn, *Appl. Phys. Lett.* **2005**, *86*, 142501-1.
- [20] H. Tanaka, J. Zhang, T. Kawai, *Phys. Rev. Lett.* **2001**, *88*, 027204-1.
- [21] F. Zavaliche, H. Zheng, L. Mohaddes-Ardabili, S. Y. Yang, Q. Zhan, P. Shafer, E. Reilly, R. Chopdekar, Y. Jia, P. Wright, D. G. Schlom, Y. Suzuki, R. Ramesh, *Nano Lett.* **2005**, *5*, 1793.
- [22] W. Eerenstein, M. Wiora, J. L. Prieto, J. F. Scott, N. D. Mathur, *Nat. Mater.* **2007**, *6*, 348.
- [23] A. Kumar, G. L. Sharma, R. S. Katiyar, R. Pirc, R. Blinc, J. F. Scott, arXiv:0812.3875v2 [cond-mat.mtrl-sci].
- [24] The critical temperature is slightly reduced in films thinner than 10 nm, see [39].
- [25] At large thicknesses, *a*-domains start to develop in the PZT layer. These ferroelectric domains are not switched under the applied electric fields used in our experiments and therefore do not contribute to the magnetoelectric effects reported here. Based on the XRD peak area, we estimate the percentage of *a*-domains to be about 5%.
- [26] The drop in magnetization for temperatures below ~90 K is due to an increase in coercivity beyond the applied field amplitude.
- [27] G. H. Jonker, J. H. van Santen, *Physica* **1950**, *16*, 337.
- [28] A. Urushibara, Y. Moritomo, T. Arima, A. Asamitsu, G. Kido, Y. Tokura, *Phys. Rev. B* **1995**, *51*, 14103.
- [29] J. Zhang, H. Tanaka, T. Kanki, J.-H. Choi, T. Kawai, *Phys. Rev. B* **2001**, *64*, 184404-1.
- [30] Z. Fang, K. Terakura, *J. Phys. Soc. Japan* **2001**, *70*, 3356.
- [31] H. Zenia, G. A. Gehring, W. M. Temmerman, *New J. Phys.* **2007**, *9*, 105-1.
- [32] M. P. de Jong, I. Bergenti, V. A. Dediu, M. Fahlman, M. Marsi, C. Taliani, *Phys. Rev. B* **2005**, *71*, 014434-1.
- [33] M. P. de Jong, I. Bergenti, W. Osikowicz, R. Friedlein, V. A. Dediu, C. Taliani, W. R. Salaneck, *Phys. Rev. B* **2006**, *73*, 052403-1.
- [34] L. D. Landau, E. M. Lifshitz, *Electrodynamics of Continuous Media*, Pergamon Press, **1960**.
- [35] C. Thiele, K. Dörr, O. Bilani, J. Rödel, L. Schultz, *Phys. Rev. B* **2007**, *75*, 054408.
- [36] We note that in Figure 3 no variations in the Kerr signal with the applied electric fields beyond the switching electric field are observed, indicating that piezoelectric and electrostrictive effects are negligible in the field range investigated. The magnetoelectric effect also persists at zero applied electric field, where electrostrictive effects can be excluded.
- [37] The MOKE measurements were taken on a time scale of minutes, much slower than the RC time constant of the system.
- [38] K. Sato, *Jap. J. Appl. Phys.* **1980**, *20*, 2403.
- [39] J. Z. Sun, D. W. Abraham, R. A. Rao, C. B. Eom, *Appl. Phys. Lett.* **1999**, *74*, 3017.